Contents lists available at ScienceDirect

Transactions of Nonferrous Metals Society of China

36(2026) 298−308

www.tnmsc.cn

Differences in competitive reactions between hydrogarnet and quicklime during Bayer digestion process

Tai-yang JI, Yi-lin WANG*, Tian-gui QI, Qiu-sheng ZHOU, Zhi-hong PENG, Gui-hua LIU, Xiao-bin LI**

School of Metallurgy and Environment, Central South University, Changsha 410083, China

Abstract: The differences in the competitive reactions of hydrogarnet and quicklime when reacting with titanium-containing and silicon-containing minerals during the Bayer digestion process were investigated. Thermodynamic analysis, artificial mineral experiments, and an evaluation of the digestion effect of natural diasporic bauxite were conducted. The results indicate that hydrogarnet shows a preferential reaction with anatase, and this preference becomes more pronounced as the silicon saturation coefficient increases. In contrast, quicklime participates in non-selective reactions with both anatase and desilication products (DSP). The preference of hydrogarnet for anatase significantly enhances the utilization efficiency of CaO in the high-temperature Bayer digestion process.

Keywords: hydrogarnet; quicklime; competitive reactions; silicon saturation coefficient; bauxite; Bayer digestion

1 Introduction

Bauxite resources in China primarily consist of diasporic bauxite [1,2]. During the Bayer digestion process, titanium-containing minerals in bauxite can form dense sodium titanate layers on the surfaces of diasporic particles. These layers can hinder the reaction of bauxite in sodium aluminate solution [3,4]. To mitigate the inhibitory effects of titanium-containing minerals, alumina refineries typically add 6%−10% quicklime [5,6]. The addition of quicklime not only alleviates these negative effects but also reduces the N/S ratio of red mud (the mass fraction ratio of Na_2O to SiO_2) and decreases the consumption of caustic alkali in the Bayer process. However, the use of quicklime presents several challenges, including increased losses of aluminum oxide [7], higher emissions of red mud, and more complex residue components. These factors collectively impede the efficient recovery of valuable elements, such as iron [8], aluminum, and titanium, from red mud.

In the Bayer process, calcium-containing phases can react with both silicon- and titanium-containing components. In sodium aluminate solutions, various thermodynamically stable or kinetically favorable phases of CaO can exist under different temperatures and alkali concentrations, such as slaked lime ($Ca(OH)_2$), calcite ($CaCO_3$), iron hydrogarnet ($3CaO{\cdot}Fe_2O_3{\cdot}nSiO_2{\cdot}(6-2n)H_2O$, n=0−1), and hydrogarnet ($3CaO{\cdot}Al_2O_3{\cdot}nSiO_2{\cdot}(6-2n)H_2O$, n=0−1). The reaction pathways that occur when these calcium-containing phases react with silicon- and titanium-containing components depend on the specific calcium-containing phase used as the initial reactant [9]. Therefore, using additives such as hydrogarnet and calcite in the Bayer digestion process can change the reaction pathways of CaO, thereby alleviating the drawbacks associated with the direct addition of quicklime. This strategy can effectively reduce the amount of

Corresponding author: *Yi-lin WANG, Tel/Fax: +86-731-88830453, E-mail: wangyilin@csu.edu.cn;
**Xiao-bin LI, Tel/Fax: +86-731-88830453, E-mail: x.b.li@csu.edu.cn

https://doi.org/10.1016/S1003-6326(25)66965-2
Received 13 May 2024; accepted 26 December 2024

CaO required while maintaining an efficient digestion process.

LI et al [10] and YANG et al [11] utilized dicalcium ferrite ($2CaO·Fe_2O_3$) as an additive for the digestion of diasporic bauxite in the Bayer process. The A/S ratio (the mass fraction ratio of Al_2O_3 to SiO_2) and the N/S ratio were less than 1.20 and 0.35 in the red mud, respectively. Furthermore, they synthesized calcium ferrite hydrate ($3CaO·Fe_2O_3·6H_2O$) as another additive, resulting in red mud with an A/S of 0.74 and an N/S of 0.24 [12]. These findings highlight the potential of dicalcium ferrite and calcium ferrite hydrate as alternatives to quicklime for enhancing alumina digestion efficiency during the Bayer process. However, it is important to note that the preparation processes for these additives are relatively complex. Dicalcium ferrite is produced by sintering iron mineral and quicklime at high temperatures, while the formation of calcium ferrite hydrate requires further hydration of dicalcium ferrite. Moreover, the addition of both additives contributes to the formation of iron hydrogarnet during the Bayer digestion process. The iron hydrogarnet can complicate the phase composition and embed characteristics of iron minerals in red mud. These changes can adversely affect the recovery of iron.

Hydrogarnet refers to a group of compounds characterized by the general chemical formula ($3CaO·Al_2O_3·nSiO_2·(6−2n)H_2O$), where n denotes the silicon saturation coefficient. Specifically, n represents the substitution degree of $4(OH)^-$ by $(SiO_4)^{4-}$ in hydrogarnet [13−15]. Thermodynamic calculations have indicated that hydrogarnet without $(SiO_4)^{4-}$ ($3CaO·Al_2O_3·6H_2O$) can react with titanium-containing minerals, resulting in the formation of perovskite ($CaTiO_3$) [16]. This reaction presents a potential solution to mitigate the retardation effects associated with titanium-containing minerals. ZENG et al [17] conducted experiments using leaf-filtered residue (38% TCA, 18% slaked lime, and 38% hydrogarnet) as a replacement for quicklime. Their results revealed that when the C/S ratio (the mass fraction ratio of CaO to SiO_2) in the configured ore was greater than 1.0, the resulting red mud exhibited an A/S ratio of less than 1.2, and the relative digestion rate of alumina surpassed 94%. Additionally, ZHANG et al [18] synthesized hydrogarnet to enhance the digestion of bauxite. The results indicated that hydrogarnet promoted digestion more effectively than quicklime when their doses were 6% CaO equivalent dosage. Under optimal conditions, the relative digestion rate of alumina surpassed 97%.

Hydrogarnet can be generated during the pre-desilication of bauxite, obtained from the desilication of crude liquor, or formed during the dealkalization of red mud. It is a byproduct of the Bayer process and presents a potential alternative to quicklime. However, current reports on the substitution of quicklime with hydrogarnet in the Bayer digestion process mainly focus on procedural discussion, while research on its reaction behavior remains limited. This study investigates the competitive reaction behaviors of hydrogarnet and quicklime with titanium- and silicon-containing minerals during Bayer digestion. The objective is to provide a fundamental explanation for the enhanced performance observed when hydrogarnet is used as a substitute for quicklime. The research involves thermodynamic calculations, artificial mineral experiments, and an evaluation of the digestion effect of natural diasporic bauxite.

2 Experimental

2.1 Materials and methods

Anatase (TiO_2, analytical reagent, ≥99%) was purchased from Sinopharm Chemical Reagent Co., Ltd. Kaolinite ($Al_2O_3·2SiO_2·2H_2O$) was a natural mineral. The diasporic bauxite used in this study (51.31% Al_2O_3, 23.30% Fe_2O_3, 5.71% SiO_2, and 3.10% TiO_2) was obtained from the Guangxi Branch of CHALCO. The mineralogical analysis identified the primary minerals of bauxite as diaspore (AlOOH), hematite (Fe_2O_3), goethite (FeO(OH)), kaolinite ($Al_2O_3·2SiO_2·2H_2O$), halloysite ($Al_2O_3·2SiO_2·4H_2O$), quartz (SiO_2), and anatase (TiO_2).

The sodium aluminate solution used in this study (232 g/L Na_2O_k, 125 g/L Al_2O_3, 10 g/L Na_2CO_3, and 5 g/L Na_2SO_4) was prepared by mixing industrial-grade aluminum hydroxide and sodium hydroxide. Na_2O_k refers to the total Na_2O equivalent concentrate of both $Na[Al(OH)_4]$ and NaOH. The desilication product (DSP) used was synthesized from kaolinite. This synthesis followed the method reported by CHENG et al [19].

The first type of hydrogarnet was obtained from the wet grinding process at an alumina plant.

The second type was sourced from the coarse liquid filtration process in the Bayer process. The third type was produced via the high-temperature digestion process of alumina. Figure 1 presents the X-ray diffraction patterns for the three samples. The silicon saturation coefficients of the samples were determined using the methods reported by LÜ et al [20] and ZHU et al [21]. For clarity and ease of explanation, the samples are designated as HG (n=0.98), HG (n=0), and HG (n=0.62), which correspond to their respective silicon saturation coefficients.

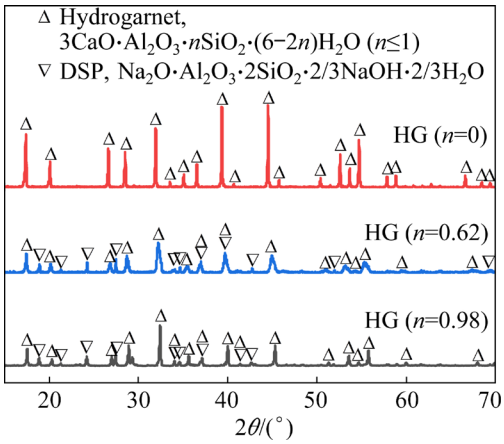

Fig. 1 X-ray diffraction patterns of hydrogarnet with different silicon saturation coefficients

In high-temperature hydrothermal experiment, the required reactants were placed into a stainless-steel bomb and mixed with a sodium aluminate solution. To facilitate mixing, three stainless-steel balls (d21 mm × 1, and d10 mm × 2) were added to the bomb. The bomb was sealed and immersed in a molten salt cell (YYL-150 × 6, Weihai Dingda Chemical Machinery Co., Ltd.) and was then rotated at 265 °C. After a designated period, the bomb was removed from the cell and promptly cooled with cold water. The resulting slurry was subsequently filtered. The filter cake was washed with hot water and dried at 100 °C for 12 h before analysis.

2.2 Characterization

The contents of Al_2O_3 and SiO_2 in red mud were analyzed using ICP-OES (iCAP PRO X, Thermofisher Scientific, America). The micro-surface morphology was observed via SEM (MIRA4 LMH, TESCAN, Czech), while the micro-area chemical components were determined using EDS (Ultim Max 40, Oxford Instruments, Britain). The XRD (Empyrean 2, PANalytical, Netherlands) analysis was conducted to identify the minerals present in the samples.

The relative digestion rates of alumina in bauxite were calculated using Eq. (1):

$$\eta_r(Al_2O_3)=\frac{(A/S)_1-(A/S)_2}{(A/S)_1-1}\times 100\% \quad (1)$$

where $\eta_r(Al_2O_3)$ denotes the relative digestion rate of alumina, while $(A/S)_1$ and $(A/S)_2$ denote the mass fraction ratios of Al_2O_3 to SiO_2 in bauxite and red mud, respectively.

3 Thermodynamic analysis

In thermodynamic calculations, the reactants included calcium-containing additives (quicklime or hydrogarnet) and main impurity minerals in bauxite (anatase and DSP). Moreover, the silicon saturation coefficients of hydrogarnet were taken as 0, 0.5, and 0.75. To get more accurate results, the thermodynamic data for hydrogarnet and DSP were estimated using the split-combination method [22,23]. Furthermore, data for other substances were obtained from Ref. [24]. In this context, Table 1 presents the possible reactions among the aforementioned reactants in the Bayer process. Meanwhile, Fig. 2 illustrates the variations in the standard Gibbs free energy change of reaction ($\Delta_rG_m^\Theta$) for these reactions from 323.15 to 573.15 K.

Figure 2(a) illustrates the variations in $\Delta_rG_m^\Theta$ during the reactions of hydrogarnet (or quicklime) with anatase at different temperatures. From 323.15 to 573.15 K, $\Delta_rG_m^\Theta$ (Nos. (1)−(4)) consistently exhibits negative values. These trends indicate that, similar to quicklime, hydrogarnet can react with anatase to form perovskite within this temperature range. Furthermore, the $\Delta_rG_m^\Theta$ (Nos. (1)−(3)) for hydrogarnet−anatase reactions shows a marked decrease with increasing temperature, whereas the $\Delta_rG_m^\Theta$ (No. (4)) for the quicklime−anatase reaction demonstrates only slight variation. Specifically, starting at approximately 432 K, the $\Delta_rG_m^\Theta$ (Nos. (1)–(3)) for the reactions of hydrogarnet with anatase becomes more negative than $\Delta_rG_m^\Theta$ (No. (4)) for the quicklime−anatase reaction, with this disparity increasing at higher temperatures. These differences suggest that the reaction of hydrogarnet with anatase is significantly more favorable than the

Table 1 Possible reactions of quicklime or hydrogarnet in Bayer digestion process

No.	Reaction
(1)	$3CaO·Al_2O_3·6H_2O+3TiO_2+2OH^-=3(CaO·TiO_2)+2[Al(OH)_4]^-+3H_2O$
(2)	$3CaO·Al_2O_3·0.5SiO_2·5H_2O+3TiO_2+1/2\ Na^++2OH^-= 3(CaO·TiO_2)+1/4(Na_2O·Al_2O_3·2SiO_2·H_2O)+3/2[Al(OH)_4]^-+11/4H_2O$
(3)	$3CaO·Al_2O_3·0.75SiO_2·4.5H_2O+3TiO_2+2OH^-+3/4Na^+= 3(CaO·TiO_2)+3/8(Na_2O·Al_2O_3·2SiO_2·H_2O)+5/4[Al(OH)_4]^-+21/8H_2O$
(4)	$CaO+TiO_2=CaO·TiO_2$
(5)	$3CaO·Al_2O_3·6H_2O+1/2(Na_2O·Al_2O_3·2SiO_2·H_2O)=3CaO·Al_2O_3·SiO_2·4H_2O+[Al(OH)_4]^-+Na^++1/2H_2O$
(6)	$3CaO·Al_2O_3·0.5SiO_2·5H_2O+1/4(Na_2O·Al_2O_3·2SiO_2·H_2O)= 3CaO·Al_2O_3·SiO_2·4H_2O+1/2[Al(OH)_4]^-+1/2Na^++1/4H_2O$
(7)	$3CaO·Al_2O_3·0.75SiO_2·4.5H_2O+1/8(Na_2O·Al_2O_3·2SiO_2·H_2O)= 3CaO·Al_2O_3·SiO_2·4H_2O+1/4[Al(OH)_4]^-+1/4Na^++1/8H_2O$
(8)	$3CaO+1/2(Na_2O·Al_2O_3·2SiO_2·H_2O)+[Al(OH)_4]^-+5/2H_2O=3CaO·Al_2O_3·SiO_2·4H_2O+Na^++2OH^-$

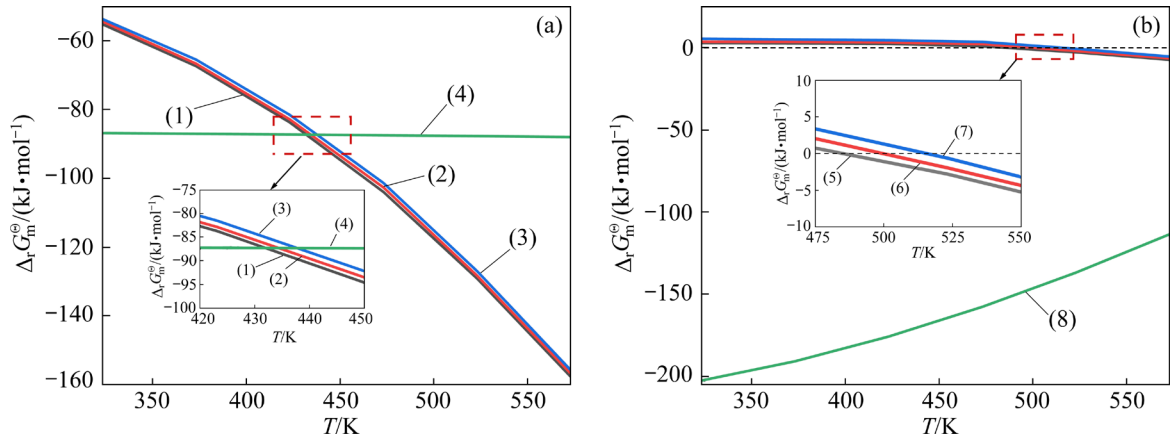

Fig. 2 Variations in $\Delta_rG_m^\Theta$ for reactions in Table 1: (a) Anatase-related reactions; (b) DSP-related reactions

quicklime−anatase reaction at the high-temperature stage of the Bayer process. Additionally, the $\Delta_rG_m^\Theta$ (Nos. (1)−(3)) can be influenced by the silicon saturation coefficients of hydrogarnet, indicating that higher silicon saturation coefficients are associated with more positive $\Delta_rG_m^\Theta$ values and higher initial temperatures at which the relevant reactions can occur.

Figures 2(b) shows the variations in $\Delta_rG_m^\Theta$ of the reactions between hydrogarnet (or quicklime) and DSP at different temperatures. At 485 K approximately, the $\Delta_rG_m^\Theta$ (No. (5)) becomes negative. Additionally, the values of $\Delta_rG_m^\Theta$ (Nos. (6) and (7)) begin to drop below zero at temperatures around 500 K and 516 K, respectively. These trends indicate a decrease in reactivity between hydrogarnet and DSP as the silicon saturation coefficient increases. Throughout the examined temperature range, the absolute values of $\Delta_rG_m^\Theta$ (Nos. (5)−(7)) remain relatively low (<7.5 kJ/mol), suggesting that the reactivity of hydrogarnet with DSP is limited. In contrast, the $\Delta_rG_m^\Theta$ (No. (8)) remains negative from 323.15 to 573.15 K, with absolute values consistently exceeding 110 kJ/mol. This highlights that, compared to hydrogarnet, quicklime exhibits a stronger propensity to engage in the dealkalization reaction with DSP throughout the Bayer process.

The comparison of Figs. 2(a) and 2(b) reveals that, at temperatures exceeding 432 K, the reaction between hydrogarnet and anatase is more probable than that between quicklime and anatase. Furthermore, as the temperature increases, the disparity between the probabilities of these two reactions becomes more pronounced. In the Bayer process, hydrogarnet only reacts with DSP at temperatures exceeding 485 K, and the difficulty of this reaction increases as the silicon saturation coefficient rises. In contrast, quicklime can react with DSP at temperatures below 373 K. The

reaction behaviors of quicklime and hydrogarnet in sodium aluminate solution reveal a significant thermodynamic discrepancy. In summary, the quicklime exhibits a lack of selectivity for titanium- and silicon-bearing minerals, whereas hydrogarnet shows a clear preference for anatase, which notably intensifies with increasing silicon saturation coefficient.

4 Results and discussion

4.1 Reactions of hydrogarnet and quicklime in high-temperature digestion

Artificial mineral experiments were carried out in both binary and ternary mineral systems to validate the results of the preceding thermodynamic analysis.

4.1.1 In binary mineral systems

2 g of calcium-containing mineral (HG (n=0.98) or quicklime) was mixed with 2 g of impurity mineral (DSP or anatase). The resulting mixture was placed in a stainless-steel bomb, to which 50 mL sodium aluminate solution was added. The bomb was then maintained at 265 °C for 60 min. Figure 3 shows the X-ray diffraction patterns of the resulting products.

Figure 3(a) displays the X-ray diffraction patterns of the product resulting from the reaction between HG (n=0.98) and DSP (or anatase). The characteristic peaks of new minerals are absent in the product resulting from the reaction of HG (n=0.98) and DSP. Moreover, the characteristic peaks of DSP remain clearly evident. This observation suggests the minimal reactivity between HG (n=0.98) and DSP during the high-temperature Bayer process. In the reaction product of HG (n=0.98) and anatase, the characteristic peaks of anatase completely disappear. Instead, high-intensity peaks corresponding to perovskite and weaker peaks associated with calcium hydroxy-titanate appear. This phenomenon indicates a significant interaction between HG (n=0.98) and anatase in the Bayer digestion process.

Figure 3(b) presents the X-ray diffraction patterns of the product obtained from the reaction between quicklime and DSP (or anatase). The characteristic peaks of hydrogarnet show up in the reaction product derived from the reaction of quicklime and DSP. This observation provides compelling evidence of a significant reaction between quicklime and DSP. Additionally, quicklime reacts with anatase to form perovskite.

Experiments on artificial minerals in binary mineral systems initially demonstrate that the hydrogarnet exhibits an obvious reaction selectivity for anatase. In contrast, the lime can undergo significant reactive processes with DSP or anatase. These findings are consistent with the thermodynamic analysis presented in Section 3.

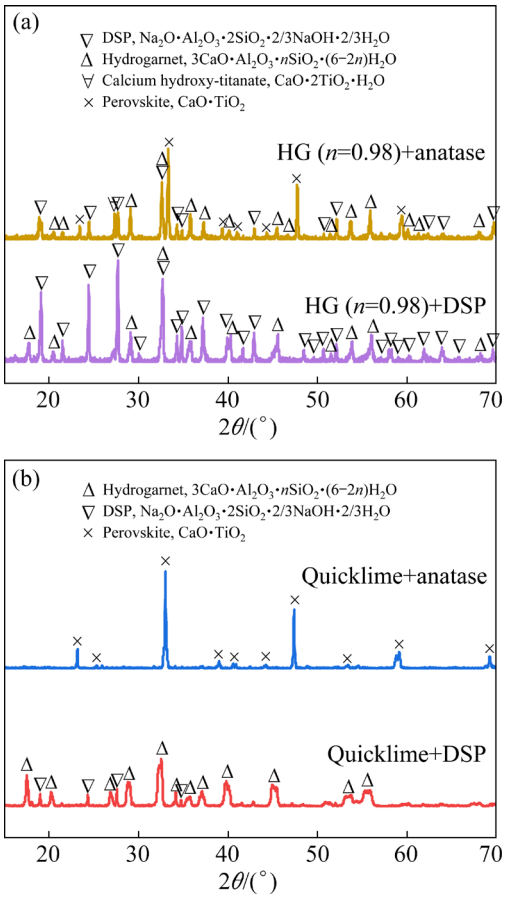

Fig. 3 X-ray diffraction patterns of products: (a) Reactants including HG (n=0.98); (b) Reactants including quicklime

4.1.2 In ternary mineral systems

Both DSP and anatase coexist in the actual Bayer process. To better investigate the differences in the reaction of hydrogarnet and quicklime when both DSP and anatase are present simultaneously, artificial mineral experiments were conducted in ternary mineral systems.

Firstly, 1 g of HG (n=0.98), HG (n=0), or quicklime was mixed with 1 g DSP and 1 g anatase. The resulting mixture was then placed into a stainless-steel bomb, to which 50.00 mL sodium aluminate solution was added. The bomb was held

at 265 °C for 30 min. Figure 4 displays the X-ray diffraction patterns of the resulting reaction products.

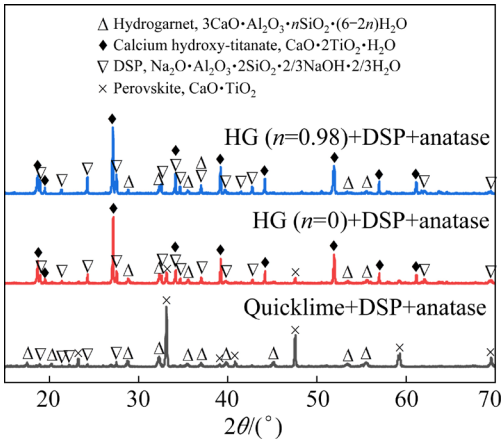

Fig. 4 X-ray diffraction patterns of products (Reactants including HG (n=0.98), HG (n=0), and quicklime)

When compared to the reaction products resulting from the reaction of quicklime, DSP, and anatase, those obtained from the reaction of hydrogarnet, DSP, and anatase exhibit significant differences. The X-ray diffraction patterns for the latter clearly display distinct characteristic peaks of unreacted DSP. In contrast, the former shows nearly absent characteristic peaks of DSP, and the peaks of hydrogarnet can be observed. Moreover, both sets of products have clear characteristic peaks of titanium-containing minerals.

Additionally, in the ternary mineral systems, the principal mineral phases in the reaction products resulting from different types of hydrogarnet demonstrate a high degree of consistency. This indicates a substantial similarity in the reaction of hydrogarnets with varying silicon saturation coefficients.

The experiments using artificial minerals conducted in ternary mineral systems provide a better representation of actual conditions than those carried out in binary mineral systems. The findings further clarify the different reactions of hydrogarnet and quicklime within the high-temperature Bayer process. Specifically, when both DSP and anatase are present simultaneously, hydrogarnet shows a highly selective reactivity toward anatase, whereas lime exhibits non-selective reactivity with both DSP and anatase. Furthermore, it is indicated that in the sodium aluminate solution, hydrogarnet with varying silicon saturation coefficients shows remarkable consistency in the reactions. The experimental results align with the conclusions drawn from the thermodynamic analysis presented in Section 3.

4.1.3 Reaction of hydrogarnet with different silicon saturation coefficients

A product was obtained from the reaction of 1 g HG (n=0.62), 1 g DSP, and 1 g anatase at 265 °C for 30 min. The X-ray diffraction pattern of this product is presented in Fig. 5.

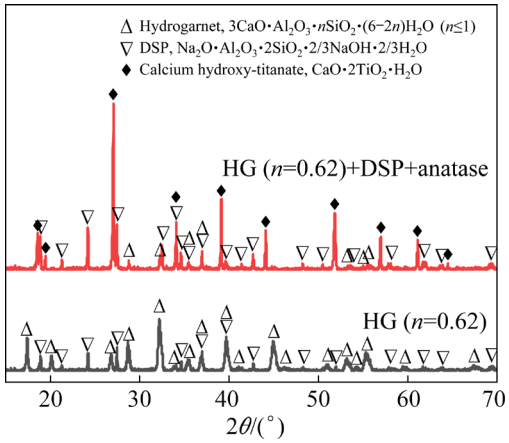

Fig. 5 X-ray diffraction pattern of HG (n=0.62) and corresponding reaction product

The silicon saturation coefficient of the initial hydrogarnet present in the reactant is 0.62, whereas that of the hydrogarnet present in the product is 0.77. This increase indicates the occurrence of a minor side reaction between the DSP and part of the initial hydrogarnet present in the reactant. However, the reaction between hydrogarnet and anatase continues to be the predominant reaction in the ternary mineral system.

To observe the differences among similar phenomena for various types of hydrogarnet, identical experiments were conducted on HG (n=0) and HG (n=0.98) under the previously specified conditions. Table 2 presents a comparison between

Table 2 Comparison of silicon saturation coefficients of hydrogarnet

Initial reactant	Coefficient of hydrogarnet in reactants	Coefficient of hydrogarnet in products	Variation of coefficients
HG (n=0)	0	0.79	0.79
HG (n=0.62)	0.62	0.77	0.15
HG (n=0.98)	0.98	0.92	−0.06

the silicon saturation coefficients of hydrogarnet present in the reactants and those present in the corresponding products.

The comparative results presented in Fig. 5 and Table 2 indicate that in the high-temperature sodium aluminate solution, most of the hydrogarnet reacts with anatase, while a smaller fraction reacts with DSP simultaneously. This portion of hydrogarnet that reacts with DSP generates new hydrogarnet with higher silicon saturation coefficients.

Furthermore, the higher the silicon saturation coefficient of hydrogarnet present in the reactants, the smaller the variation of the coefficient in Table 2. This suggests that the reaction difficulty between hydrogarnet and DSP is positively correlated with the silicon saturation coefficient of hydrogarnet itself. For HG (n=0.98) with a silicon saturation coefficient close to 1, the hydrogarnet present in the corresponding product exhibits a decreased silicon saturation coefficient. This phenomenon is likely attributable to the partial dissolution of silicon from HG (n=0.98) into the sodium aluminate solution at elevated temperatures, although the reaction between HG (n=0.98) and DSP is relatively weak.

4.2 Mechanism of hydrogarnet reaction process

In the binary mineral systems, 1 g HG (n=0.98) was mixed with 1 g anatase and subsequently immersed in 50 mL sodium aluminate solution. The reactions were conducted at 265 °C for 5, 20, and 60 min, respectively. Figure 6 illustrates the microscopic morphology of the products at various reaction time. Table 3 presents the results of the EDS analysis, detailing the chemical compositions of the selected micro-regions depicted in Fig. 6.

The analysis reveals that the rapid reaction between HG (n=0.98) and anatase at 265 °C initially produces calcium hydroxy-titanate, which is characterized by a regularly hexagonal plate structure. The calcium hydroxy-titanate exhibits smooth surfaces, the particle sizes range from 5 to 7 μm, and the molar ratios of TiO_2 to CaO are approximately 2.0. As the reaction progresses, the surfaces of calcium hydroxy-titanate gradually dissolve or undergo structural fracturing. These transformations facilitate the formation and growth of hemispherical particles, for which the molar ratios of TiO_2 to CaO range from 1.3 to 1.8. The final products of the reaction are numerous spherical perovskite particles with diameters less than 1 μm. These observations confirm that the

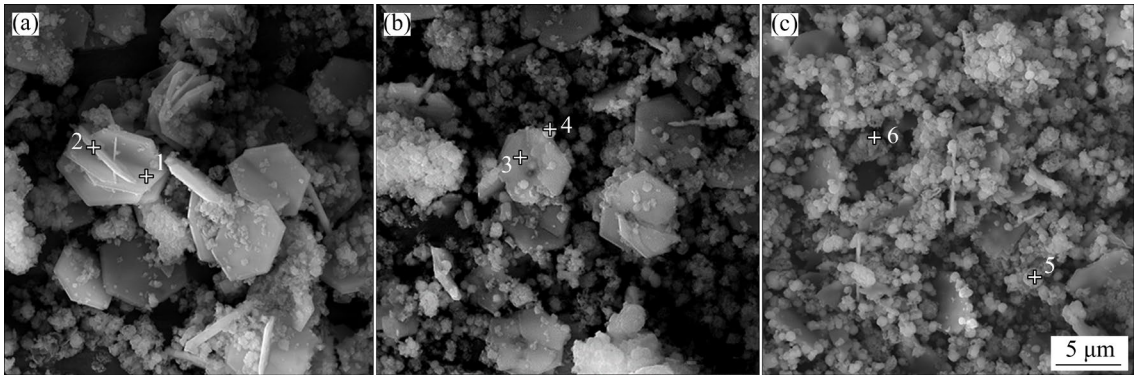

Fig. 6 Microscopic morphology of products at various reaction time: (a) 5 min; (b) 20 min; (c) 60 min

Table 3 Chemical compositions of selected micro-regions in Fig. 6

Region No.	Chemical composition/at.%					TiO_2/CaO	Na_2O/CaO	Al_2O_3/CaO	SiO_2/CaO
	CaO	TiO_2	Na_2O	Al_2O_3	SiO_2				
1	10.62	22.15	1.24	1.34	1.19	2.09	0.12	0.13	0.11
2	7.34	14.85	1.19	1.12	0.62	2.02	0.16	0.15	0.08
3	8.37	14.34	2.59	2.22	2.96	1.71	0.31	0.27	0.35
4	8.51	11.72	3.21	1.80	3.21	1.38	0.38	0.21	0.38
5	8.69	9.44	4.09	2.96	6.08	1.09	0.47	0.34	0.70
6	8.18	8.60	2.54	2.67	5.75	1.05	0.31	0.33	0.70

formation of perovskite through the reaction between hydrogarnet and anatase is relatively slow in the Bayer process.

In the ternary mineral system, a reaction involving 1 g HG (n=0.98), 1 g DSP, and 1 g anatase was conducted in the sodium aluminate solution at 265 °C for 30 min. Figure 7 illustrates the microscopic morphology and chemical components of reactants and products as examined through SEM and EDS.

Figure 7(a) illustrates microscopic morphology of a mixture containing HG (n=0.98), DSP, and anatase.

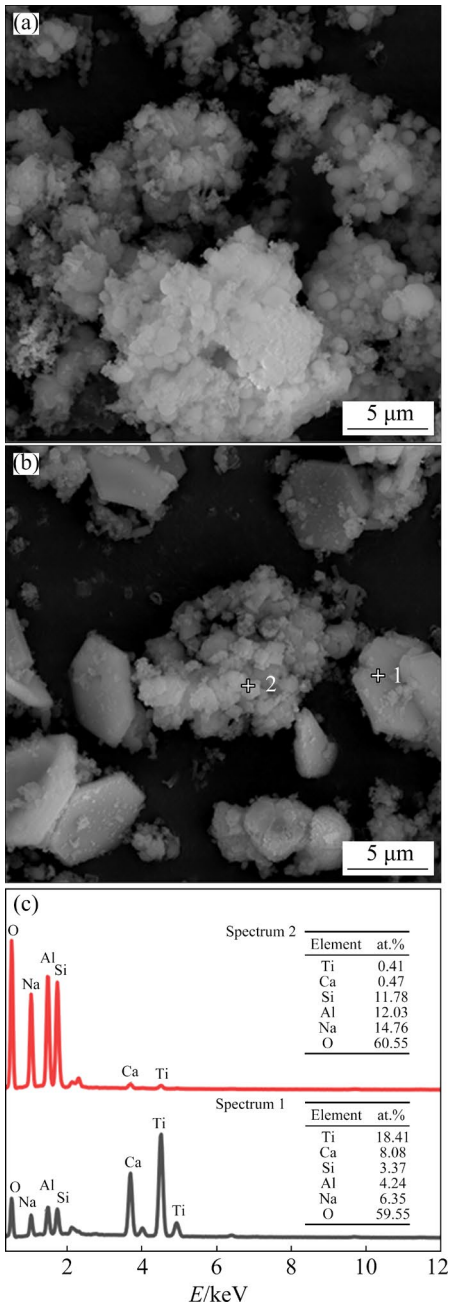

Fig. 7 Microscopic morphology and chemical components of (a) reactants and (b, c) products

The image reveals irregular blocky aggregates, spherical particles with an average diameter of approximately 1 μm, and a notable presence of sub-spherical particles measuring less than 0.2 μm.

Figure 7(b) exhibits microscopic morphology of the products. Numerous complete regular hexagonal plate particles (calcium hydroxy-titanate) are displayed. The diameters of these particles range from 5 to 7 μm, closely resembling those found in binary mineral systems. Additionally, irregular blocky aggregates with approximate diameters of 15 μm exist in the product. The EDS analysis reveals that the principal chemical components of these aggregates are Si, Al, and Na, with minimal quantities of Ca and Ti. Therefore, it can be concluded that these irregular blocky aggregates, which exhibit limited participation in reactions, are identified as DSP.

4.3 Evaluation of digestion effects on natural diasporic bauxite

To evaluate the differences in the promoting effects of hydrogarnet and quicklime on the digestion of natural bauxite, 26.71 g diasporic bauxite was mixed with quicklime, HG (n=0.98), or HG (n=0), respectively. The dosages of these additives were classified into three levels (2%, 4%, and 7%) based on their ratios to the mass of bauxite. Subsequently, these mixtures were placed into stainless-steel bombs containing 100 mL sodium aluminate solution. Bombs were then maintained at 265 °C for 70 min. Figure 8 illustrates the results of the digestion process.

Figure 8(a) shows that, at the same actual dosages, hydrogarnet has a more pronounced promoting effect on bauxite digestion compared to quicklime. Meanwhile, Fig. 8(b) demonstrates that, during a limited digestion period and at identical CaO equivalent dosages, the relative digestion rates of alumina with the addition of hydrogarnet are significantly higher than those of alumina with the addition of quicklime. Figure 9 presents the best digestion results under the optimal conditions in the Bayer process. When the CaO equivalent dosage of quicklime is 7.00%, the relative digestion rate of alumina reaches 95.01%. In contrast, with a CaO equivalent dosage of HG (n=0.98) at 2.81%, the relative digestion rate of alumina increases to 99.98%. The observations from experiments on the

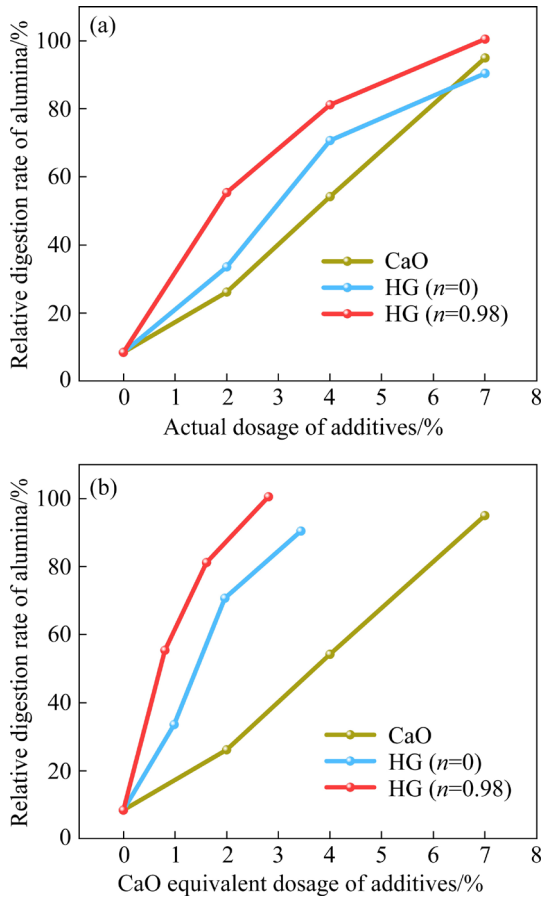

Fig. 8 Relative digestion rates of alumina with different additives: (a) Actual dosage; (b) CaO equivalent dosage

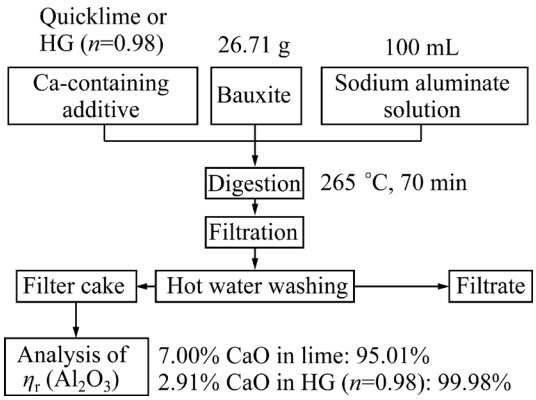

Fig. 9 Relative digestion rates of alumina ($\eta_r(Al_2O_3)$) under optimal conditions

digestion of natural diasporic bauxite confirm that, given a limited digestion time and an identical CaO equivalent dosage, CaO in hydrogarnet shows significantly higher utilization efficiency compared to CaO in quicklime. This provides robust support for the thermodynamic analysis and the results of the artificial mineral experiments presented in the preceding sections.

At the same CaO equivalent dosages, the relative digestion rates of alumina are higher when HG (n=0.98) is added compared to HG (n=0). For instance, when the CaO equivalent dosage is 1.96%, the relative digestion rate of alumina with HG (n=0.98) added exceeds 82.00%, whereas the relative digestion rate of alumina with HG (n=0) added is only 70.71%. This finding indicates that in the digestion of natural diasporic bauxite, hydrogarnet with silicon saturation coefficients approaching the upper limit (n=1) exhibits minimal reactivity with DSP as well, and this specific reactivity enhances its effectiveness in promoting bauxite digestion. In contrast, similar to the experiments using artificial minerals, although hydrogarnet with low silicon saturation coefficients primarily interacts with anatase, a smaller portion can engage in a weak reaction with the DSP synchronously, resulting in a slightly weaker promotion effect on diasporic bauxite digestion.

5 Conclusions

(1) Thermodynamic calculations suggest that both hydrogarnet and quicklime can react with anatase during the Bayer process. The reaction trend of hydrogarnet with anatase surpasses that of quicklime with anatase at 432 K, and the disparity becomes increasingly pronounced as the temperature rises. Quicklime significantly inclines to react with DSP throughout the entire process. In contrast, hydrogarnet displays a weaker tendency to react with DSP only above 485 K. Furthermore, an increase in the silicon saturation coefficient decreases the probability of reaction between hydrogarnet and DSP.

(2) In artificial mineral experiments, quicklime can react simultaneously with both anatase and DSP without showing any preference. In contrast, hydrogarnet demonstrates a distinct tendency to react with anatase. This selective difference leads to the CaO in hydrogarnet exhibiting a superior digestion-promoting ability compared to the CaO in quicklime. Under the optimal conditions for natural bauxite digestion experiments, using 2.81% CaO equivalent dosage of HG (n=0.98) achieves a relative alumina digestion rate of 99.98%. However, when 7.00% CaO equivalent dosage of quicklime is added, the relative digestion rate of alumina merely reaches 95.01%.

(3) In the Bayer process, hydrogarnet with silicon saturation coefficients near the upper limit (n=1) exhibits minimal reactivity with DSP. Instead, although hydrogarnet with low silicon saturation coefficients preferentially reacts with titanium-bearing minerals, a smaller proportion concurrently reacts with DSP, thereby resulting in the formation of hydrogarnet with higher silicon saturation coefficients. Consequently, the higher silicon saturation coefficient in hydrogarnet leads to a more pronounced enhancement in digestion. In natural bauxite digestion experiments, at the same CaO equivalent dosage, the relative alumina digestion rate with HG (n=0.98) added is 11.29% higher than that with HG (n=0) added.

CRediT authorship contribution statement

Tai-yang JI: Methodology, Software, Data curation, Investigation, Writing – Original draft; **Yi-lin WANG:** Conceptualization, Methodology, Validation, Writing – Review & editing, Funding acquisition, Supervision; **Tian-gui QI:** Writing – Review & editing; **Qiu-sheng ZHOU:** Investigation, Writing – Review & editing; **Zhi-hong PENG:** Writing – Review & editing; **Gui-hua LIU:** Writing – Review & editing; **Xiao-bin LI:** Conceptualization, Methodology, Supervision, Writing – Review & editing.

Declaration of competing interest

The authors declare that they have no known competing financial interests or personal relationships that could have appeared to influence the work reported in this paper.

Acknowledgments

The authors gratefully appreciate the financial support from the Natural Science Foundation of Hunan Province, China (No. 2022JJ40616).

References

[1] SUN Li, ZHANG Shuai, ZHANG Shi-hong, LIU Jian-nan, XIAO Ke-yan. Geologic characteristics and potential of bauxite in China [J]. Ore Geology Reviews, 2020, 120: 103278.

[2] GAO Lan, LI Ji-hong, WANG Deng-hong, XIONG Xiao-yun, YI Cheng-wei, HAN Mei-zhi. Outline of metallogenic regularity of bauxite deposits in china [J]. Acta Geologica Sinica (English Edition), 2015, 89(6): 2072−2084.

[3] LI Xiao-bin, YU Shun-wen, LIU Nan, CHEN Yong-kun, QI Tian-gui, ZHOU Qiu-sheng, LIU Gui-hua, PENG Zhi-hong. Dissolution behavior of sodium titanate in sodium aluminate solutions at elevated temperatures [J]. Hydrometallurgy, 2014, 147/148: 73−78.

[4] ZHOU Guo-tao, WANG Yi-lin, QI Tian-gui, ZHOU Qiu-sheng, LIU Gui-hua, PENG Zhi-hong, LI Xiao-bin. Comparison of the effects of Ti- and Si-containing minerals on goethite transformation in the Bayer digestion of goethitic bauxite [J]. International Journal of Minerals, Metallurgy and Materials, 2023, 30(9): 1705−1715.

[5] LI Xiao-bin, FU Wei-an, ZHOU Qiu-sheng, LIU Gui-hua, PENG Zhi-hong. Reaction behavior and mechanism of anatase in digestion process of diasporic bauxite [J]. Transactions of Nonferrous Metals Society of China, 2010, 20(1): 142−146.

[6] LI Xiao-bin, WANG Yi-lin, ZHOU Qiu-sheng, QI Tian-gui, LIU Gui-hua, PENG Zhi-hong, WANG Hong-yang. Transformation of hematite in diasporic bauxite during reductive Bayer digestion and recovery of iron [J]. Transactions of Nonferrous Metals Society of China, 2017, 27(12): 2715−2726.

[7] LI Li-li, WU Ze-gang, LV Han, LIU Feng-qin, ZHAO Hong-liang. Reaction behavior of aluminogoethite and silica minerals in gibbsite bauxite in high-temperature digestion [J]. Journal of Sustainable Metallurgy, 2022, 8(1): 360−369.

[8] ZHOU Guo-tao, WANG Yi-lin, QI Tian-gui, ZHOU Qiu-sheng, LIU Gui-hua, PENG Zhi-hong, LI Xiao-bin. Enhanced conversion mechanism of Al-goethite in Gibbsitic bauxite under reductive Bayer digestion process [J]. Transactions of Nonferrous Metals Society of China, 2022, 32(9): 3077−3087.

[9] SMITH P. Reactions of lime under high temperature Bayer digestion conditions [J]. Hydrometallurgy, 2017, 170: 16−23.

[10] LI Xin-hua, GU Song-qing, YIN Zhong-lin, WU Guo-bao, WANG Ya-dong, ZHAI Yu-chun. Digesting rule and mechanism of middle and low grade bauxite with calcium ferrite [J]. The Chinese Journal of Nonferrous Metals, 2008, 18: 101−105. (in Chinese)

[11] YANG Fan, ZHANG Tao, XIE Gang, SHI Yu-sheng. Effect of dissolution performance of bauxite by different additives in Bayer process [J]. Nonferrous Metals Engineering, 2018, 8(6): 51−55. (in Chinese)

[12] LI Xin-hua, GU Song-qing, YIN Zhong-lin, WANG Ya-dong, WU Guo-Bao, ZHAI Yu-chun. Regulation and mechanism study on new Bayer process-additive hydro calcium ferrite [J]. Nonferrous Metals (Extractive Metallurgy), 2008(6): 18−21. (in Chinese)

[13] MAEDA H, KUROSAKI Y, NAKAMURA T, NAKAYAMA M, ISHIDA E H., KASUGA T. Control of chemical composition of hydrogrossular prepared by hydrothermal reaction [J]. Materials Letters, 2014, 131: 132−134.

[14] MAEDA H, MINOWA S, URUSHIHARA D, ASAKA T. Controlling the chemical composition of garnet with hydroxy groups for humic acid removal [J]. Ceramics International, 2023, 49(7): 11107−11111.

[15] MINOWA S, MAEDA H. Preparation of hydrogarnet/poly (lactic acid) composite adsorbents for humic substance removal [J]. MATERIALS, 2022, 16(1): 336.

[16] LI Xiao-bin, ZHOU Qiu-sheng, WANG Hao-yu, PENG Zhi-hong, LIU Gui-hua. Hydrothermal formation and conversion of calcium titanate species in the system Na_2O−

Al_2O_3−CaO−TiO_2−H_2O [J]. Hydrometallurgy, 2010, 104(2): 156−161.

[17] ZENG Xian-fei, ZHANG Tian-xing, ZHANG Shun-fei. Application research on hydrated calcium aluminate by Bayer's process [J]. Light Metals, 2021(11): 26−29. (in Chinese)

[18] ZHANG Lun-he, XU Qi-li, WANG Xiang-li. Effect of different additives in diasporic bauxite during Bayer digestion [J]. Light Metals, 1995(7): 9−14. (in Chinese)

[19] CHENG Lu- wei, WANG Yi-lin, WANG Biao, QI Tian-gui, LIU Gui-hua, ZHOU Qiu-sheng, PENG Zhi-hong, LI Xiao-bin. Phase transformation of desilication products in red mud dealkalization process [J]. Journal of Sustainable Metallurgy, 2022, 8(1): 541−550.

[20] LÜ Guo-zhi, ZHANG Ting-an, ZHU Xiao-feng, ZHENG Chao-zhen, WANG Yan-xiu, ZHANG Wei-guang, ZHANG Zi-mu. Silicon saturation coefficient changes in hydrogarnets during the Bayer process with lime addition [J]. Chinese Journal of Chemical Engineering, 2019, 27(8): 1965−1972.

[21] ZHU Xiao-feng, LIU Yong-mei, JIANG Feng-qi, LI Bin, LV Guo-zhi, ZHANG Ting-an. Calcification-carbonation method for bayer red mud treatment: Carbonation performance of hydrogarnets [J]. Bulletin of Environmental Contamination and Toxicology, 2022, 109(1): 68−75.

[22] LI Xiao-bin, YANG Li-qun, ZHOU Qiu-sheng, QI Tian-gui, LIU Gui-Hua, PENG Zhi-hong. A split-combination method for estimating the thermodynamic properties ($G_f^{\ominus}$ and $H_f^{\ominus}$) of multicomponent minerals [J]. Applied Clay Science, 2020, 185: 105406.

[23] LI Xiao-bin, LI Yong-fang, LIU Xiang-min, LIU Gui-hua, PENG Zhi-hong, ZHAI Yu-chun. A simple method of estimation of Gibbs free energy and enthalpy of complicate silicates [J]. Journal of the Chinese Ceramic Society, 2001, 29(3): 232−237. (in Chinese)

[24] YANG Xian-wan, HE Ai-ping, YUAN Bao-zhou. Calculation Handbook of thermodynamic data for high-temperature aqueous solution [M]. Beijing: Metallurgical Industry Press, 1983: 47−694. (in Chinese)

拜耳法溶出过程中水化石榴石和生石灰竞争反应的差异

计太阳，王一霖，齐天贵，周秋生，彭志宏，刘桂华，李小斌

中南大学 冶金与环境学院，长沙 410083

摘　要：研究了拜耳法溶出过程中水化石榴石和生石灰与含钛、含硅矿物反应时竞争反应的差异。采用热力学分析、人工矿物实验和天然一水硬铝石型铝土矿消化效果评价等方法进行分析。结果表明，水化石榴石显示出与锐钛矿的优先反应，并且这种偏好随着硅饱和系数的增加而变得更加明显。相比之下，生石灰同时参与锐钛矿和脱硅产物(DSP)的非选择性反应。水化石榴石对锐钛矿的偏好显著提高了高温拜耳法溶出过程中 CaO 的利用效率。

关键词：水化石榴石；生石灰；竞争反应；硅饱和系数；铝土矿；拜耳法溶出

(Edited by Bing YANG)